Geochimica et Cosmochimica Acta 344 (2023) 146–159

Contents lists available at ScienceDirect

Geochimica et Cosmochimica Acta

journal homepage: www.elsevier.com/locate/gca

Origin of the superchondritic carbon/nitrogen ratio of the bulk silicate Earth – an outlook from iron meteorites

Damanveer S. Grewal *, Paul D. Asimow

Division of Geological and Planetary Sciences, California Institute of Technology, 1200 E California Blvd, Pasadena, CA 91125, USA

ARTICLE INFO

Article history:
Received 20 September 2022
Accepted 13 January 2023
Available online 20 January 2023
Associate editor: Mathieu Roskosz

Keywords:
Carbon
Nitrogen
Iron meteorites
Planetesimals
Planet formation

ABSTRACT

Disagreement regarding the origin of the bulk silicate Earth's (BSE) superchondritic carbon/nitrogen (C/N) ratio is due, in part, to the unknown C/N ratios of differentiated planetesimals – the building blocks of Earth-like rocky planets. In this study we report solid–liquid metal partitioning experiments for C and N that allow us to reconstruct, from the C and N contents of iron meteorites, the C/N ratios of the cores of the earliest formed planetesimals. Due to their siderophile character, most of the C and N retained in these bodies after differentiation resides in their cores. Therefore, estimates of the bulk C and N contents and C/N ratios of the cores yield confident estimates of these quantities in the complete parent bodies of iron meteorites. Our experimental data, at 1 GPa and 1200–1400 °C, show that C and N are incompatible in solid metal relative to S-poor liquids but compatible in solid metal relative to S-rich liquids. Crucially, N is approximately an order of magnitude more compatible than C in S-rich systems. S itself is incompatible in solid metal and so the late-crystallizing liquids persisting at the end of core freezing were S-rich for most cores. Although these late-crystallizing liquids are unsampled by iron meteorites, we infer that their N contents and C/N ratios were generally lower and higher, respectively, than those in iron meteorites. Depending upon the fraction of unsampled late-crystallizing liquids as well as their S contents, the C/N ratios of the bulk cores and complete parent bodies are either similar to or higher than those measured in iron meteorites. The reconstructed C/N ratios of most of the parent bodies of iron meteorites are chondritic, except that the volatile-rich IC and IIC groups have superchondritic C/N ratios. Importantly, the C/N ratio of the parent body of the IC iron meteorite group lies within the estimated range of the BSE, whereas the C/N ratios of all other groups are lower. Correlated depletion of moderately volatile elements like Ge and Ga with C and N, variations in metallographic cooling rates, and Pd-Ag isotope systematics suggest that the parent cores of the volatile-depleted iron meteorite groups were likely affected by volatile degassing. If volatile-rich iron meteorite groups like the IC better capture the C and N inventories of the parent cores of the earliest formed planetesimals, then delivery of C and N via such planetesimals makes the superchondritic C/N ratio of the BSE a natural consequence of the Earth's accretion history. Otherwise, poorly constrained processes like atmospheric erosion or C and N delivery by exotic materials are required to explain the superchondritic C/N ratio of the BSE.

1. Introduction

The storage and exchange of carbon (C) and nitrogen (N) among the reservoirs of the bulk silicate Earth (BSE = surface fluid envelopes + crust + mantle) controls the long-term climate of our planet (Zahnle et al., 2007; Gaillard and Scaillet, 2014; Grewal et al., 2020; Gaillard et al., 2021). Tracing the origin of the present-day inventory of these life-essential volatiles in the BSE is therefore key to understanding the formation of habitable worlds in our Solar System and beyond. Despite considerable research, the absolute concentrations of C and N in the BSE, especially the mantle, are not easily constrained and are somewhat model dependent (Marty and Zimmermann, 1999; Marty, 2012; Halliday, 2013; Hirschmann, 2018; Marty et al., 2020). By comparison, the comparable geochemical characteristics of these two elements (e.g., incompatible behavior during partial melting and low solubility in silicate melts) makes C/N ratio a widely used tracer of the origin of volatiles in the BSE (Marty, 2012; Halliday, 2013; Bergin et al., 2015; Hirschmann, 2016; Marty et al., 2020). However, the most up-to-date estimates of the C inventory of the mantle differ by a factor of four, resulting in estimates of the C/N ratio

* Corresponding author.
E-mail address: dgrewal@caltech.edu (D.S. Grewal).

https://doi.org/10.1016/j.gca.2023.01.012
0016-7037/

of the BSE of 50 by Hirschmann (2018) and 190 by Marty et al. (2020). The merits of the approaches followed by each study to estimate the C content of the BSE are well established. Without preferring one estimate over the other, we have used C/N ratios from both studies for discussion in this study.

As C and N are siderophile and atmophile elements, their BSE inventories are biased towards the later stages of Earth's accretion (e.g., the Moon forming impact and late accretion) (Hirschmann, 2016; Dasgupta and Grewal, 2019; Grewal et al., 2021b). Comparisons between the C/N ratios of the BSE and cosmochemical reservoirs yield important constraints on the timing and mode of C and N delivery to Earth (e.g., Bergin et al., 2015; Grewal et al., 2019b; Hirschmann, 2016; Sakuraba et al., 2021). $^{13}C/^{12}C$ and $^{15}N/^{14}N$ ratios suggest that the Earth and meteorite parent bodies inherited C and N from common precursors (Alexander et al., 2012; Grewal et al., 2021c; Marty, 2012). Mean C/N ratios of chondrites, regardless of the growth zone of their parent bodies in the protosolar disk, are lower than that of the BSE. For example, mean C/N ratios of enstatite and carbonaceous chondrites (ECs and CCs, the best representatives of primitive materials of inner and outer Solar System origin, respectively) vary between 12 and 26 (Grewal et al., 2019b). Only ordinary chondrites (OCs) exhibit slightly higher C/N ratios, but it remains uncertain whether the C/N ratios of OCs are known well enough – due to the low concentrations of both elements in OCs approaching the detection limits of the best analytical methods (Hirschmann, 2016) – to represent their parent bodies. Also, the practical difficulties in generating homogenous powders for the analyses of OCs (due to the presence of variable amounts of C- and *N*-rich metals (Hashizume and Sugiura, 1995, 1997)), results in substantial variation in their C/N ratios. Therefore, we have avoided using the C/N ratios of OCs for comparison in this study. The observation that the C/N ratio of the BSE is higher than that of chondrites (i.e., superchondritic) makes the delivery of C and N to the BSE directly via chondrite-like materials unlikely (Marty, 2012; Hirschmann, 2016). Extensive research effort has been directed at seeking to understand the cause(s) of the superchondritic C/N ratio of the BSE. Preferential segregation of N into the core was put forward as a possibility, yielding a superchondritic C/N ratio in the BSE despite a chondritic ratio in the whole Earth (BSE + core) (Marty, 2012; Roskosz et al., 2013). However, experimental data have shown that N is not substantially more siderophile than C over a wide range of core formation scenarios applicable to Earth's growth (Hirschmann, 2016; Dalou et al., 2017; Grewal et al., 2019a; Dasgupta and Grewal, 2019). An alternate solution is impact erosion of N-rich atmosphere(s) during Earth's growth (Tucker and Mukhopadhyay, 2014; Sakuraba et al., 2021; Chen and Jacobson, 2022). However, this model cannot explain the subchondritic $N/^{36}Ar$ ratio of the BSE because erosion of atmosphere(s) containing N and Ar, which have similar degassing efficiencies, should have resulted in a chondritic $N/^{36}Ar$ in the BSE (Marty and Zimmermann, 1999; Marty et al., 2020). Only a fortuitous combination of atmosphere erosion and core segregation in sequence could fit both the C/N and $N/^{36}Ar$ constraints, but the dynamics of impact erosion of atmospheres and their effect on volatile loss are too uncertain to develop well-constrained tests of such a hybrid model.

Another class of alternative explanations call for delivery of the entire C and N inventories of the present-day BSE via materials with superchondritic C/N ratios towards the tail-end of Earth's accretion. Suggestions include thermally metamorphosed CV-CO chondrites (Marty et al., 2020), ureilites (Hirschmann, 2016), or a Mars-sized planetary embryo with a graphite-saturated core (Grewal et al., 2019b). However, the superchondritic C/N ratio of CV and CO chondrites assumed by Marty et al. (2020) stems from the extremely low N abundances reported by Kerridge (1985). Pearson et al. (2006) measured the same samples (which are all falls) as Kerridge (1985) and reported N concentrations an order of magnitude higher, resulting in chondritic C/N ratios for the CV and CO groups. Alexander et al. (2012) verified the higher N contents and chondritic C/N ratios in CV and CO chondrites by measuring samples which were chiefly finds from Antarctica. Therefore, even though it is still not clear whether the high N abundances measured by Kerridge (1985) or the low N abundances obtained by Pearson et al. (2006) are more representative of CV and CO falls, the relatively low N contents in CV and CO finds measured by Alexander et al. (2012) casts doubt on the hypothesis that these groups had superchondritic C/N ratios. In the case of ureilites, it is likely that their C-rich nature was not a primitive signature of their parent body but rather the result of a late stage infiltration of C-rich fluids or melts into the mantle residues (sampled by these meteorites) after the segregation of silicate and Fe-Ni-S melts (Day et al., 2017). On the other hand, even though the accretion of an impactor with a graphite-saturated core can deliver the C and N budget of the BSE with a superchondritic C/N ratio (Grewal et al., 2019b), the hypothesis is currently *ad-hoc* and cannot be independently verified by other means.

The idea that the superchondritic C/N ratio of the BSE is in fact a problem requiring one of the above hypotheses, however, rests on the premise that chondrite-like materials were the direct building blocks of rocky planets. There is a central drawback to this premise. Planet formation models combined with chronological constraints from meteorites indicate rapid growth of planetesimals at the onset of Solar System formation (Kruijer et al., 2014; Morbidelli et al., 2022). These early planetesimals incorporated substantial amounts of short-lived radionuclides (primarily ^{26}Al) whose decay led to large-scale melting and differentiation (Hevey and Sanders, 2006; Sahijpal et al., 2007). Therefore, it is likely that differentiated planetesimals rather than chondrite-like undifferentiated materials were the building blocks of the larger rocky bodies of the Solar System. In fact, paleomagnetic data and thermochemical models for CV, CM, and Rumuriti chondrites suggest that many, if not all, groups of chondrites originate from the surficial layers of mostly differentiated planetesimals rather than from entirely undifferentiated bodies (Elkins-Tanton et al., 2011; Weiss and Elkins-Tanton, 2013). Such differentiation would be associated with partial and probably differential depletion of volatile elements, such that the C/N ratios of the cores (which retain sizeable C and N inventories (Hirschmann et al., 2021; Grewal et al., 2021c, 2021a, 2022b)) and mantles of the differentiated planetesimals could be markedly different from those of the undifferentiated surficial regolith sampled by chondrites. It follows one cannot safely assume that the C/N ratios of chondrites define the initial condition for the C/N ratio of the rocky planets. Such as assumption could lead to an entirely unnecessary level of complexity in planet formation models and, in any case, the assumption must be tested.

In this study, we present an alternate approach in understanding the relationship between the C/N ratio of the present-day BSE and its building blocks. We use the C and N abundances of magmatic iron meteorites (Fig. 1) – remnants of the metallic cores of differentiated planetesimals (Goldstein et al., 2009) – to infer the bulk C/N ratios of their parent bodies. Using iron meteorites as a proxy to track the C/N ratio of the building blocks of the Earth presents several clear advantages. Iron meteorites sample the earliest formed planetesimals in the Solar System, having accreted as early as ~0.1 Ma after CAIs (Calcium-Aluminum-rich Inclusions, the solids that date 'time zero' of Solar System formation) (Kruijer et al., 2017), whereas chondrites sample planetesimals that accreted rather late, i.e., ~2–4 Ma after CAIs (Sugiura and Fujiya, 2014). As planet formation models predict that the seeds of rocky planets grew within ~1–2 Ma after CAIs (Morbidelli et al., 2022), iron meteorites are a better proxy for the C/N ratio of the building blocks of the Earth. Also, the grouped magmatic iron meteorites

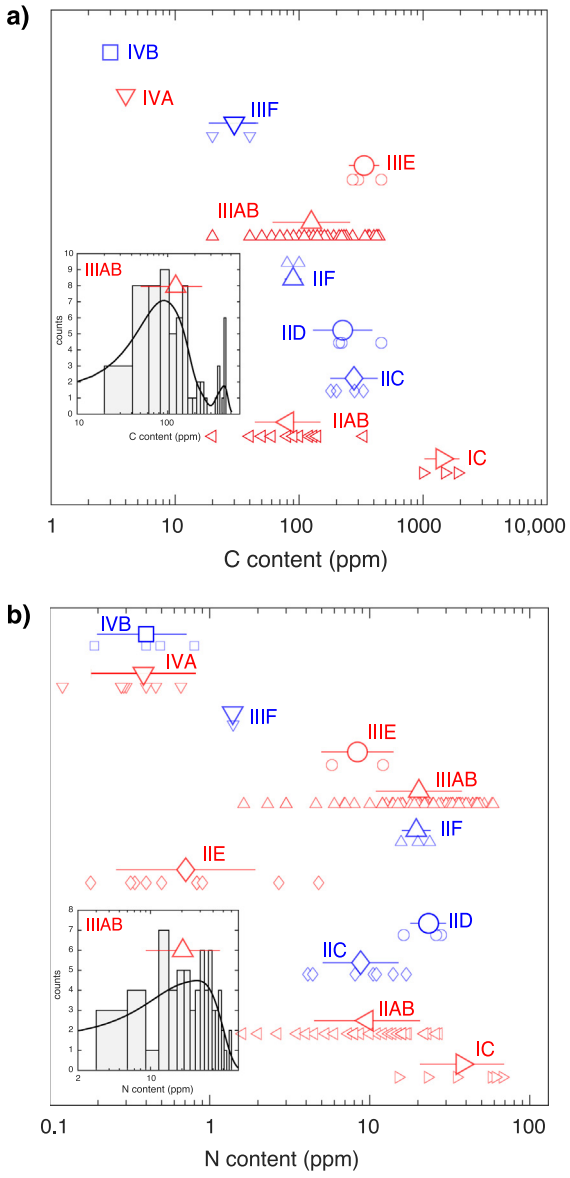

Fig. 1. Distribution of (a) C and (b) N contents (smaller symbols) in iron meteorites along with the geometric mean values (larger symbols) and 1 standard deviation (s.d.) from the geometric mean for each group. Log-normal kernel density estimates (made with MATLAB® software) of C and N contents of IIIAB iron meteorite groups are also shown in the inset for comparison. Iron meteorite groups are plotted in red and blue colours based on their non-carbonaceous (NC; inner Solar System) or carbonaceous (CC; outer Solar System) reservoir heritage (Kruijer et al., 2017). Data sources: C – (Moore et al., 1969; Lewis and Moore, 1971; Buchwald, 1975; Goldstein et al., 2017); N – (Gibson and Moore, 1971; Kothari and Goel, 1974; Shukla and Goel, 1981; Murty et al., 1983; Franchi et al., 1993; Prombo and Clayton, 1993; Mathew et al., 2000; Ponganis and Marti, 2007). Refer to the supplementary section for details related to the measurements of C and N in iron meteorites. (For interpretation of the references to colour in this figure legend, the reader is referred to the web version of this article.)

sample multiple planetesimals (10 in total) from the inner and outer regions of the protosolar disk (Kruijer et al., 2017). Therefore, they sample the C/N ratios of a planetesimals covering a wide range of growth zones. Provided C/N ratios of the parent cores can be estimated for each group of iron meteorites, bulk C/N ratios of the parent bodies can be constrained using the C/N ratios of the cores in tandem with metal-silicate partition coefficients for C ($D_C^{metal/silicate}$) and N ($D_N^{metal/silicate}$). Bulk C/N ratios of differentiated planetesimals can then be compared with that of the BSE to evaluate the origin of C and N in the Earth.

2. Methods

2.1. Estimating carbon and nitrogen contents of the parent cores from iron meteorites

Magmatic iron meteorites sample cores which were once fully molten (Goldstein et al., 2009) and subsequently underwent fractional crystallization, resulting in characteristic correlations among siderophile trace elements such As, Au, and Ir (Chabot and Jones, 2003; Chabot, 2004). Hence, elemental concentrations in iron meteorite samples are used in conjunction with fractional crystallization models to estimate the inventories of trace elements in the parent cores of magmatic irons (Chabot and Zhang, 2022; Zhang et al., 2022). However, C and N abundances in magmatic irons are uncorrelated with indices of fractional crystallization (Supplementary Fig. 1). While this may indicate that C and N contents of a parent core can be directly estimated from individual samples within a group without placing them in a fractional crystallization sequence (Hirschmann et al., 2021; Grewal et al., 2022a), there is a caveat to this approach. Fractional crystallization models for multiple trace elements indicate that samples representing the conjugate liquids remaining towards the end of the fractionation sequence are missing for all magmatic iron groups (Hilton et al., 2022; Chabot and Zhang, 2022; Zhang et al., 2022). These conjugate liquids must have been S-rich for almost all magmatic iron meteorite groups, though in detail the S content of the missing conjugate liquids depend upon the initial S content of each parent core and the extent of the fractional crystallization sequence that is unsampled (Chabot and Zhang, 2022). It may be that either magmatic irons do not capture the entire fractional crystallization sequence or that fractional crystallization ceased (due to early disruption of the parent bodies) before reaching the Fe-Ni-S eutectic (Chabot and Zhang, 2022). In either case, the iron meteorite collection would be an incomplete sample of the bulk composition of the initial core liquid.

Previous experimental studies show that the activity coefficients of C and N in metallic melts increase substantially with increasing S contents (Tsuno et al., 2018; Grewal et al., 2019b, 2019a). Therefore, it is possible that the residual S-rich liquids had notably different C and N contents than earlier crystallized solids, in which case the C and N concentrations in iron meteorite samples from a given group cannot be used to directly estimate the C and N inventories of the parent cores. This is true even though C and N do not correlate with indices of fractional crystallization across the range sampled by the iron meteorites. It may be that the evolution of their partition coefficients was such that C and N did not begin to diverge from their parent core concentration until the liquid became more S-rich than the sampled population. It may also be the case that sub-solidus redistribution of C and N has wiped out the original correlations. For an element to show coherent fractional crystallization trends, its inventory in each incrementally solidified layer should remain locked post-crystallization, i.e., its diffusion across the solidified layers must be minimal (Campbell and Humayun, 2005; Chabot and Zhang, 2022). The diffusion coefficients of C and N in solid metal are ~3–4 orders of magnitude higher than the trace elements that do show coherent fractional crystallization trends (Oikawa, 1982). For instance, C and N would diffuse in solid metal by ~0.1 m/yr at 800 °C whereas Au, Ir, and Ga diffuse by ~0.001 m/yr. Thus the lack of correlation between C and N concentrations and extent of fractionation in sampled iron meteorites does not imply that their budgets and ratio in the parental core liquids can be directly measured; the parameters of the fractionation process must still be considered. It should be noted that even though absolute concentrations of C and N are variable within a given group of iron

meteorites (probably due to shock and deformation-induced diffusion during disruption of their parent cores (Franchi et al., 1993)), the mean concentrations of C and N are correlated with each other (Fig. 1; see Supplementary Section for details). Also, the mean concentrations of C and N across all groups of iron meteorites are correlated with the volatile depletion index defined by the concentrations of Ge and Ga. For example, the IC group is the most Ge- and Ga-rich as well as C- and N-rich group of iron meteorites, whereas the IVA and IVB groups form a low-concentration end-member for Ge and Ga and also for C and N. Hence, it is very likely that, as with the MVEs, the mean concentrations of C and N in a given group of magmatic iron meteorites inform us about the C and N concentrations in the sampled portions of their parent cores.

Limited theoretical and experimental data examining the partitioning of C between solid and liquid iron (both for S-bearing and S-free systems) hint at substantial fractionation between the two phases. Hirschmann et al. (2021) employed thermodynamic calculations (based on 1 atm metallurgy data) to determine $D_C^{solid/liquid}$ (the partition coefficient of C between solid and liquid metal) by matching the activity of C in equilibrating solid Fe—C metal and Fe—C—S liquid. This model predicts that $D_C^{solid/liquid}$ should increase from ~0.1 to 100 as the S content of the liquid metal increases from 0 to 30 wt%. No experimental study has yet characterized the effect of S in liquid metal on $D_C^{solid/liquid}$ at the elevated pressures relevant to core crystallization in planetesimals. Moreover, the effect of S in liquid metal on $D_N^{solid/liquid}$ (the partition coefficient of N between solid and liquid metal) is completely unknown. To comprehensively constrain $D_C^{solid/liquid}$ and $D_N^{solid/liquid}$ values as a function of S content of the metallic melts, we experimentally equilibrated solid and liquid metal at elevated pressures (P) and temperatures (T). The experimental data is combined with the C and N contents of iron meteorites and the estimated missing portions of the fractional crystallization sequences to constrain the bulk C and N inventories and C/N ratios of the parent cores for each group of iron meteorites.

2.2. Details of high pressure-high temperature experiments

2.2.1. Starting compositions

The metallic mixtures were composed of variable amounts of Fe, Ni, S, C, and N. Reagent grade Fe, Ni, Fe_3N, and vitreous C were mixed with or without elemental S to synthesize starting mixtures (0S = 0 wt% S, 3S = 3 wt% S, 8S = 8 wt% S) (Supplementary Table 1). Within the T range of our experiments, the use of three different starting mixtures allowed us to constrain the partitioning of C and N between solid and liquid metal with a range of 0–28 wt% S in the liquid phase. Following several previous studies (e.g., Chabot et al., 2017, 2006), Ni content was fixed at 10 wt% to capture the compositional range of the parent cores of most iron meteorite groups. The reagent grade powders were homogenized by mixing in an agate mortar under ethanol for ~1 h and dried overnight.

2.2.2. Experimental details

The sizes of the parent cores of iron meteorites are not fully constrained. Metallographic cooling rates of iron meteorites suggest that the parent cores of some groups had radii ranging from 70 to 150 km (Yang et al., 2007, 2008, 2010). Core-mass fractions of 0.14–0.22 (Hilton et al., 2022) would result in parent body radii ranging from 300 to 500 km. Self-gravitation calculations show that core crystallization in the center of these bodies would take place at pressures closer to 1 GPa than 1 atm. Therefore, experiments of this study were performed at 1 GPa and at temperatures between 1200 and 1400 °C. It should be noted that there is evidence for cooling of some cores occurred without insulating mantles (based on the inverse correlations between cooling rates and Ni contents (Yang et al., 2007)). In that case, core crystallization would likely have taken place at pressures lower than that explored in this study. The experiments were conducted in an end-loaded piston cylinder device at Caltech utilizing ½ inch CaF_2-crushable MgO assemblies and straight-walled graphite heaters following the calibrations and procedural details of previous studies from the same lab (e.g., Weidendorfer and Asimow, 2022). Due to the relatively inert behavior of MgO towards solid and liquid metals, we used crushable MgO capsules to load our starting materials. Temperature was monitored using a $W_{95}Re_5$-$W_{74}Re_{26}$ thermocouple (C-type) with no pressure correction on the electromotive force. A stream of industrial nitrogen gas was introduced at the top of the upper cooling plate where the W-Re wires emerged to prevent their oxidation during the course of the experiment. The loaded assemblages were pressed cold to 1 GPa followed by isobaric heating at a rate of 100 °C/min. The experiments were sintered overnight at 850 °C followed by heating to the target temperature. The sintering step is essential to reduce the porosity and permeability of MgO capsule and prevent leakage of alloy melts or diffusion of C—N bearing vapor across the capsule walls (Grewal et al., 2021b, 2021a). The experiments were quenched isobarically by cutting the heating power. After depressurization, the recovered samples were cut longitudinally using a 30 μm thick diamond blade. The cut samples were mounted in Crystalbond™, ground with 1200 grit SiC, and then polished with 0.3 μm alumina slurry. Crystalbond™ was removed from the polished sample by soaking overnight in acetone.

2.2.3. Analytical details

The compositions of the coexisting solid and liquid metals were measured using an electron probe micro-analyzer (JEOL JXA 8200) at Caltech. We used uncoated experimental products and standards due to their conductive nature. Accounting for the heterogenous texture of the quenched metallic melts, especially those containing S, 50–100 μm beams were used to obtain representative bulk metallic melt compositions. Pure Fe and Ni metal were used as standards for Fe and Ni X-ray intensity. Natural troilite (FeS) was used as a standard for S. Fe_3C and Fe_3N standards for C and N were synthesized by following the protocol of previous studies (Dasgupta and Walker, 2008; Grewal et al., 2019b). An accelerating voltage of 12 kV and an emission current of 80nA allows simultaneous measurement of C and N K_α X-rays with an LDE2 diffracting crystal (Grewal et al. 2019b, 2019a, 2021b, 2021a). For all elements except N, a counting time of 10 s on peak and 5 s each at lower and upper background positions was used. A counting time of 80 s on peak and 60 s at each background position was used for N. Fe and FeS standards were re-analyzed after every ~20 measurements to check for C deposition on standards and samples during the analysis. C blank in the standards did not increase with time, and remained constant at ~0.4–0.5 wt% as reported in several previous studies (e.g., Tsuno et al., 2018; Grewal et al., 2019b, a). The reported C concentrations in the solid and liquid metals are corrected values, obtained by subtracting the relevant C blanks in the Fe and FeS standards.

3. Results

3.1. Texture of experimental products

The solid and liquid metals co-existed as two well-separated phases in the quenched products (Fig. 2a). For a given starting mixture, the volume of the liquid phase increased with an increase in temperature. The solid metal was present as a single homogenous

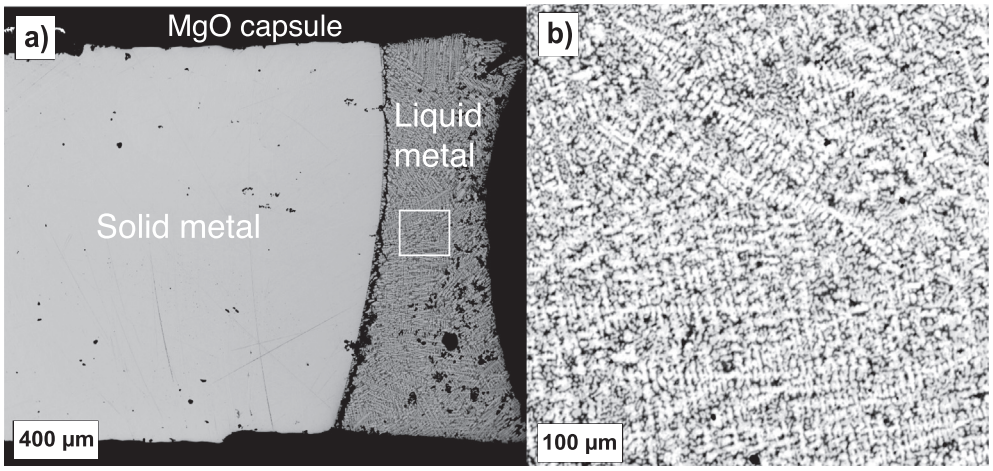

Fig. 2. Backscattered electron images of a typical experimental product (Expt. no. R551 containing ~15 wt% S in the liquid) displaying the co-existence of solid and quenched liquid metals. (a) Solid (Fe, Ni) metal was homogenous, whereas liquid metal quenched to a dendritic texture. (b) Enlargement of the white boxed area in (a), displaying the typical quenched texture after a S-bearing metallic melt; a 50–100 μm diameter beam is sufficient to obtain an average liquid composition from this quench aggregate.

phase. As reported in several previous studies (Chabot and Drake, 1997; Chabot et al., 2003, 2009), the liquid metal, though a single homogenous phase at the target temperature, quenched to a dendritic texture (Fig. 2b) composed of elongated, branching Fe-Ni crystals surrounded by interstitial Fe carbides, Fe nitrides, and FeS (in S-bearing mixes). No pre-quench or post-quench accessory C phases were observed in any of the experimental products.

3.2. Experimental results on the partition coefficients of C and N between solid and liquid metals

The compositions of the solid and liquid metals are reported in Supplementary Tables 2 and 3. The solid metal/liquid metal weight ratio partition coefficients of C ($D_C^{solid/liquid}$) and N ($D_N^{solid/liquid}$) are reported in Table 1. Both $D_C^{solid/liquid}$ and $D_N^{solid/liquid}$ increase with increasing S content of the metallic melts (Fig. 3a). Carbon is incompatible in the solid metal at less than ~20 wt% S in the metallic melt whereas N is incompatible at less than ~15 wt% S. $D_C^{solid/liquid}$ is lower than $D_N^{solid/liquid}$ for the entire range of S contents explored in this study. The difference between $D_C^{solid/liquid}$ and $D_N^{solid/liquid}$ is not substantial for metallic melts containing less than ~11 wt% S but becomes larger for S-rich melts. For example, $D_N^{solid/liquid}$ is almost an order of magnitude higher than $D_C^{solid/liquid}$ for the most S-rich metallic melts (~28 wt% S) explored in this study. For S-poor metallic melts, $D_C^{solid/liquid}$ values from this study are within the range of the theoretical predictions of Hirschmann et al. (2021) (Fig. 3a). However, the present $D_C^{solid/liquid}$ measurements increase more gently with increasing S content that the prediction of Hirschmann et al. (2021), with the difference amounting to more than an order of magnitude in the most S-rich compositions studied. However, $D_C^{solid/liquid}$ values based on C contents in Fe_3C and S-rich melts at 2 GPa (from the phase equilibrium study of the Fe—C—S ternary) by Dasgupta et al. (2009) lie within the range of experimental data of this study.

As reported in several previous studies (e.g., Chabot, 2004; Chabot et al., 2009; Chabot and Drake, 1997), the S content of the metallic melt and temperature are intertwined. The experimental data of this study is not sufficient to systematically constrain the effect of temperature on $D_C^{solid/liquid}$ and $D_N^{solid/liquid}$ for S-bearing metallic melts. The three experiments conducted at different temperatures for S-free systems show that both $D_C^{solid/liquid}$ and $D_N^{solid/liquid}$ decrease with increasing temperature (Fig. 3b), but the change in both partition coefficients as a function of temperature is much less than their variation as a function of S content of the metallic melts. It should be noted that the $D_C^{solid/liquid}$ for S-free systems observed here is well within the range of experimental data on the Fe-Ni-C system at 1 atm (Chabot et al., 2006) and the Fe-C system at 5 GPa (Chabot et al., 2008).

Table 1
Summary of experimental conditions, quench products, and solid–liquid metal partition coefficients of carbon and nitrogen.

Exp Samples	P (GPa)	T (°C)	Duration (h)	Starting compositions	Capsule	Quench Products	$D_C^{solid/liquid}$		$D_N^{solid/liquid}$	
							Mean	1-σ	Mean	1-σ
R551	1	1200	8	Fe-10Ni-0.5C-1N-3S	MgO	Solid metal + Liquid metal	0.71	0.23	1.04	0.14
R574	1	1250	6	Fe-10Ni-0.5C-1N-3S	MgO	Solid metal + Liquid metal	0.61	0.20	0.67	0.21
R566	1	1275	6	Fe-10Ni-0.5C-1N-3S	MgO	Solid metal + Liquid metal	0.55	0.16	0.61	0.15
R550	1	1300	6	Fe-10Ni-0.5C-1N-3S	MgO	Solid metal + Liquid metal	0.54	0.11	0.56	0.11
R552	1	1350	6	Fe-10Ni-0.5C-1N-3S	MgO	Solid metal + Liquid metal	0.58	0.12	0.57	0.06
R560	1	1400	7	Fe-10Ni-0.5C-1N-3S	MgO	Solid metal + Liquid metal	0.54	0.17	0.58	0.09
R573	1	1200	6	Fe-10Ni-1C-1.5N-8S	MgO	Solid metal + Liquid metal	2.64	0.38	17.93	1.80
R558	1	1250	8.5	Fe-10Ni-1C-1.5N-8S	MgO	Solid metal + Liquid metal	1.91	0.17	4.93	0.28
R571	1	1275	6	Fe-10Ni-1C-1.5N-8S	MgO	Solid metal + Liquid metal	0.93	0.13	2.47	0.18
R556	1	1300	6.5	Fe-10Ni-1C-1.5N-8S	MgO	Solid metal + Liquid metal	0.68	0.08	0.91	0.12
R557	1	1350	6	Fe-10Ni-1C-1.5N-8S	MgO	Solid metal + Liquid metal	0.64	0.14	0.66	0.08
R569	1	1300	6	Fe-10Ni-0.5C-1N-0S	MgO	Solid metal + Liquid metal	0.48	0.11	0.67	0.11
R568	1	1350	6	Fe-10Ni-0.5C-1N-0S	MgO	Solid metal + Liquid metal	0.45	0.12	0.62	0.18
R561	1	1400	6	Fe-10Ni-0.5C-1N-0S	MgO	Solid metal + Liquid metal	0.40	0.12	0.57	0.18

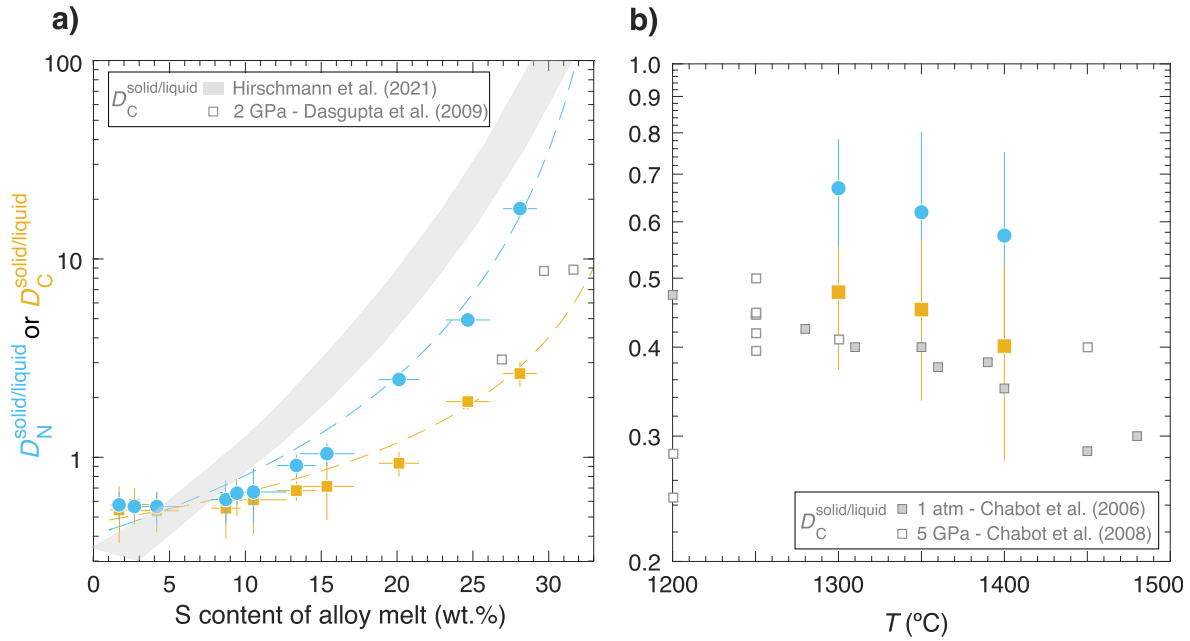

Fig. 3. $D_C^{solid/liquid}$ and $D_N^{solid/liquid}$ as a function of (a) S content of the metallic melt and (b) temperature (for S-free starting mixtures). (a) $D_C^{solid/liquid}$ and $D_N^{solid/liquid}$ increase by ~1 and 2 orders of magnitude, respectively, with increasing S content of the metallic melts. Carbon and nitrogen transition from incompatible to compatible behavior at ~20 and 15 wt% S in the metallic melt. The parametrized fits for $D_C^{solid/liquid}$ and $D_N^{solid/liquid}$ using Eqs. (3) and (4), respectively, are shown by dashed lines. $D_C^{solid/liquid}$ values in this study are approximately an order of magnitude lower than the theoretical predictions of Hirschmann et al. (2021) at 1 atm and 1300 °C. $D_C^{solid/liquid}$ values determined from phase relations in the Fe—C—S ternary by Dasgupta et al. (2009) at 2 GPa lie within the range of experimental data of this study. (b) For S-free systems, $D_C^{solid/liquid}$ and $D_N^{solid/liquid}$ decrease with increasing temperature. $D_C^{solid/liquid}$ from this study are well within the range of the experimental data of Chabot et al. (2006) at 1 atm and Chabot et al. (2008) at 5 GPa. Error bars for $D_C^{solid/liquid}$, $D_N^{solid/liquid}$, and S content in this study represent ± 1σ deviation obtained by the propagation of uncertainty from the standard deviation of replicate analyses of C, N, and S contents. Where absent, the error bars are smaller than the symbol size.

There are several indirect lines of evidence that point to the achievement of equilibrium partitioning of C and N between solid and liquid metals in our experiments. No compositional gradients were observed in either solid or liquid for any analyzed element. Given the fast diffusivity of C and N in metallic solids and liquids in the temperature range of our experiments (on the order of 10^{-8} m^2s^{-1} (Oikawa, 1982)), both C and N should attain compositional homogeneity over the mm scale of our experimental capsules within a few minutes. Exploring the Fe-C phase diagram at 5 GPa and 1250 °C, Chabot et al. (2008) showed that equilibrium distribution of C between Fe_3C and metallic melt is established in less than 30 min. All experiments in this study had a runtime of ~6 h or greater. Moreover, the S-free $D_C^{solid/liquid}$ results in this study lie well within the range of 1 atm experiments conducted by Chabot et al. (2006) with durations of 12–144 h (Fig. 3b).

3.3. Parameterizations of the partition coefficients of C and N between solid and liquid metals

In the Fe-Ni-S system explored in this study, C and N exhibit a behavior typical of numerous siderophile elements like As, Au, Co, Mo, Ni, Rh, Ru, Sb, and Sn – incompatible in the solid metal relative to S-free or S-poor liquid metals and becoming increasingly compatible in solid metal as the S content of the liquid metal increases (Fig. 3a). Therefore, we adopted the framework that Chabot and Jones (2003) developed for parameterizing solid/liquid metal partition coefficients of other siderophile trace elements. For each element i (C and N in this case), $D_i^{solid/liquid}$ is calculated based on the equation:

$$\ln(D_i) = \ln(D_{i0}) + \beta \ln(\text{Fe domains}) \quad (1)$$

where D_{i0} is the partition coefficient between solid and liquid metal in a S-free, Fe-Ni system; β is a constant determined by the regression fit; and "Fe domains" is defined as the fraction of free S atoms present in the liquid metal, given by:

$$\text{Fe domains} = \frac{1 - 2X_S}{1 - X_S} \quad (2)$$

where X_S represents the mole fraction of S in the liquid metal.

Using this framework, linear regression in $\ln(D_i)$ vs "Fe domains" yields the following best-fit parameterizations:

$$\ln\left(D_C^{solid/liquid}\right) = -0.75(\pm 0.05) - 1.51(\pm 0.10).\ln(\text{Fe domains}) \quad (3)$$

$$\ln(D_N^{solid/liquid}) = -0.90(\pm 0.07) - 3.17(\pm 0.15).\ln(\text{Fe domains}) \quad (4)$$

The regression lines for $D_C^{solid/liquid}$ and $D_N^{solid/liquid}$ are compared with the experimental data in Supplementary Fig. 2, which also gives 95 % confidence bounds and correlation coefficients of the regressions. The parametrized fits for $D_C^{solid/liquid}$ and $D_N^{solid/liquid}$ using Eqs. (3) and (4) are plotted in Fig. 3a.

4. Discussion

Our experimental data show that C and N (like many siderophile elements) increasingly partition into the solid metal as the S content of the metallic melt increases, becoming moderately compatible for C and highly compatible for N. However, $D_C^{solid/liquid}$ values in this study, especially for S-rich metallic melts, are substantially lower than the theoretical predictions of Hirschmann et al. (2021) (Fig. 3a). The discrepancy could be a direct result of pressure (a parameter that is known to affect Fe—C—S phase relations; Chabot et al., 2008; Dasgupta et al., 2009)). Hirschmann et al. (2021) used 1 atm experimental data for Fe-Ni-C taenite (Wada

et al., 1971) and Fe—C—S melts (Wang et al., 1991) in their thermodynamic models, whereas the data in this study were collected at 1 GPa. $D_C^{solid/liquid}$ values for S-rich melts, determined from the phase relations of the Fe—C—S ternary at 2 GPa by Dasgupta et al. (2009) are more similar to the results of this study. Core crystallization beneath insulating mantles must have taken place at pressures that are closer to 1 GPa than 1 atm. Another possible source of the discrepancy is the effect of Ni; Hirschmann et al. (2021) used data from for Ni-free metal liquids, whereas the parent cores of all iron meteorites contained Ni (Hilton et al., 2022). Whether the difference is due to pressure or Ni content, this study determined $D_C^{solid/liquid}$ under conditions more relevant to the fate of C during solidification of the parent cores of iron meteorites.

We also note that, despite the variable amounts of C and N in the two S-bearing mixtures of this study, $D_C^{solid/liquid}$ and $D_N^{solid/liquid}$ each follow systematic correlations with S contents of the metallic melts (Fig. 3a). Thus, the observed partitioning of C and N between solid and liquid metals appears to be consistent with the Nernst distribution law (Henrian behavior in both solid and liquid phases) within the range of C and N contents explored.

For S-rich metallic melts, we find that $D_N^{solid/liquid}$ is considerably higher than $D_C^{solid/liquid}$ (Fig. 3a). Consequently, equilibration of S-rich metallic melts with solid metal should manifest in substantial fractionation between C and N. This observation has important implications for the bulk C/N ratios of the parent cores because the missing portions of the parent cores for most groups of magmatic irons were composed of S-rich melts (Hilton et al., 2022; Chabot and Zhang, 2022; Zhang et al., 2022). In the next subsection we use the $D_C^{solid/liquid}$ and $D_N^{solid/liquid}$ fits obtained in this study to estimate the C and N contents of the missing portions of all groups of magmatic irons. These estimated values are used to constrain the bulk C and N inventories as well as the C/N ratios of the parent cores and parent bodies of iron meteorites.

4.1. Estimating bulk C and N contents and C/N ratios of the parent cores of iron meteorites

As C and N fractionate between solid and liquid metal, their concentrations in samples of a given group of iron meteorites cannot be used to directly estimate C and N contents of the parent cores. Carbon and nitrogen concentrations in samples from magmatic iron groups, however, do not exhibit correlations with indices of fractional crystallization (Supplementary Fig. 1). Therefore, unlike other siderophile elements (Hilton et al., 2022; Chabot and Zhang, 2022; Zhang et al., 2022), fractional crystallization models cannot be used to estimate the bulk C and N inventories of the parent cores of magmatic irons from observed elemental concentrations in iron meteorite samples. Hence, we propose an alternate approach. First, we use C and N concentrations in iron meteorite samples to estimate geometric mean C and N contents in the sampled fractions of the core for the parent body of each group (Fig. 1; Table 2). Then, the missing mass fraction from the end of the crystallization sequence of each parent core (Hilton et al., 2022; Chabot and Zhang, 2022; Zhang et al., 2022; Tornabene et al., 2023) is combined with the S content of the parent core (Chabot, 2004; Hilton et al., 2022) to quantify the S content of the missing conjugate liquid for each group of magmatic irons. The S content is inserted into the parametrized $D_C^{solid/liquid}$

Table 2
Carbon and nitrogen concentrations and C/N ratios in iron meteorites, unsampled fractions of the cores, parent cores, and parent bodies.

Groups	Iron Meteorites		Unsampled Cores		Parent Cores		Parent Bodies	
	ln C (ppm)	1-σ	ln C (ppm)	1-σ	ln C (ppm)	1-σ	ln C (ppm)	1-σ
IC	7.26	0.32	6.98	0.29	7.02	0.44	5.50	0.60
IIAB	4.39	0.61	3.02	0.15	3.91	0.63	2.42	0.75
IIC	5.41	0.55	5.80	0.23	5.70	0.60	3.99	0.73
IID	5.62	0.44	5.92	0.28	5.87	0.52	3.91	0.67
IIF	4.49	0.16	3.12	0.07	4.15	0.17	2.21	0.45
IIIAB	4.83	0.72	4.00	0.18	4.55	0.74	3.00	0.85
IIIF	3.34	0.49	3.22	0.69	3.31	0.84	1.60	0.94
IVA	1.39	–	1.27	0.67	1.35	0.67	−0.30	0.19
IVB	1.10	–	1.71	0.13	1.27	0.13	−1.94	0.44
Groups	**Iron Meteorites**		**Unsampled Cores**		**Parent Cores**		**Parent Bodies**	
	ln N (ppm)	1-σ	ln N (ppm)	1-σ	ln N (ppm)	1-σ	ln N (ppm)	1-σ
IC	3.63	0.61	2.36	0.18	2.64	0.63	1.18	0.70
IIAB	2.26	0.76	−1.31	0.34	1.58	0.83	0.13	0.10
IIC	2.17	0.55	2.29	0.76	2.26	0.93	0.59	0.36
IID	3.13	0.29	3.06	0.53	3.07	0.61	1.18	0.62
IIF	2.97	0.21	−0.60	0.07	2.50	0.22	0.61	0.37
IIIAB	3.01	0.62	0.57	0.21	2.50	0.65	0.98	0.72
IIIF	0.34	–	−0.60	0.09	0.17	0.09	−1.50	0.31
IVA	−1.15	0.50	−2.09	0.44	−1.35	0.66	−2.97	0.73
IVB	−0.88	0.60	−0.29	0.70	−0.71	0.92	−3.77	0.96
Groups	**Iron Meteorites**		**Unsampled Cores**		**Parent Cores**		**Parent Bodies**	
	ln C/N	1-σ	ln C/N	1-σ	ln C/N	1-σ	ln C/N	1-σ
IC	3.63	0.17	4.62	0.09	4.37	0.25	4.32	0.60
IIAB	2.13	0.36	4.33	0.26	2.33	0.55	2.29	0.78
IIC	3.45	0.27	3.50	0.33	3.44	0.43	3.40	0.63
IID	2.29	0.12	2.86	0.18	2.79	0.22	2.74	0.55
IIF	1.52	0.08	3.72	0.13	1.65	0.10	1.60	0.64
IIIAB	1.82	0.25	3.43	0.37	2.05	0.31	2.01	0.78
IIIF	3.01	0.15	3.82	0.26	3.14	0.60	3.10	0.62
IVA	2.54	0.43	3.36	0.57	2.71	0.70	2.67	0.68
IVB	1.98	0.68	1.99	0.84	1.98	0.59	1.83	0.34

and $D_N^{solid/liquid}$ equations (Eqs. (3) and (4)) to predict C and N contents of the conjugate liquid, i.e., in the unsampled portion of the parent core (Fig. 4; Table 2). Finally, the sampled and predicted C and N concentrations and the mass fractions of the sampled and unsampled portions are combined to estimate the bulk C and N inventories of each parent core (Fig. 5; Table 2). A comparable approach was applied by Hirschmann et al. (2021) to estimate the C contents of the coexisting conjugate liquids. But Hirschmann et al. (2021) did not combine the C concentrations of the coexisting solids and conjugate liquids with the relative fractions of sampled and missing portions of cores to estimate the bulk C inventories of the parent cores.

As $D_C^{solid/liquid}$ values are closer to unity (Fig. 3a), C concentrations in the missing fractions of the cores are not substantially different from the sampled fractions (Fig. 4a; Table 2). However, $D_N^{solid/liquid}$ achieves notably greater values for S-rich metallic melts (Fig. 3a), leading to estimated N concentrations in the S-rich missing fractions that are substantially lower than the sampled fractions (Fig. 4b; Table 2). This leads to estimated bulk C concentrations in the parent cores that are similar to those measured in the iron meteorites, whereas bulk N concentrations in the parent cores (especially those with more S-rich missing portions) are lower than those measured in iron meteorites (Fig. 5a; Table 2). We note that C and N concentrations in the parent cores do not show any systematic difference between groups with non-carbonaceous (NC) or carbonaceous (CC) reservoir heritage. This observation is in contrast to the N isotopic signatures of iron meteorites; the NC irons have systematically lower $^{15}N/^{14}N$ ratios than the CC irons. The IC group parent core has the highest C and N contents, whereas the IVA and IVB groups have the lowest (Fig. 5a). This observation is in agreement with the volatile depletion trend observed for moderately volatile elements (MVEs) like Ge and Ga where IC group are MVE-rich and IVA and IVG groups are MVE-depleted (Goldstein et al., 2009).

C/N ratios of the missing fractions of the cores (especially those with more S-rich missing fractions) are higher than those of the sampled fractions (Fig. 4c; Table 2). Due to the high S content of its parent core (~19 wt%; Hilton et al. (2022)) and a large fraction of missing core in the meteorite record, the C/N ratio of the parent core of IC group is substantially higher than the iron meteorites samples from that group. Consequently, reconstructed bulk C/N ratios in the parent cores of all magmatic iron groups are generally higher than the mean C/N ratios (that is, the ratio of the geometric mean concentration of C to than of N) of meteorite samples of the respective groups (Fig. 5b; Table 2). Mean C/N ratio of the parent core of volatile-rich IC group is considerably higher than the mean C/N ratios of other volatile-depleted groups. As with their C and N contents, the C/N ratios of the parent cores do not systematically differ between groups with NC and CC reservoir heritage.

The framework of our calculations assumes that iron meteorites sample pure taenite cumulates crystalized from metallic melts without any pockets of trapped liquid. However, the fractionation trends of some groups of iron meteorites are better explained by models that incorporate some fraction of trapped melt crystallization (Wasson, 1999; Chabot and Zhang, 2022). For example, magmatic CC irons are predicted to contain small fractions of trapped melts (x <0.15) whereas some NC iron groups can contain larger fractions. For these groups, the application of a melt-free pure taenite cumulate model is not completely valid. If the trapped melts were depleted in C and N relative to taenite (because $D_C^{solid/liquid}$ and $D_N^{solid/liquid}$ > 1), then the melt-crystal aggregate would have less C and N than the pure cumulate model. Hence, our calculations underestimate the C and N contents in the conjugate liquids by a factor of 1–x, where 'x' is the fraction of trapped melt. There is also an error in C/N ratios due to trapped melt, since $D_C^{solid/liquid} \neq D_N^{solid/liquid}$, but the assumption about melt-free cumulates is only applied to the sampled part of the fractionation sequence, where S contents are low and the difference between the partition coefficients is small.

4.2. Estimating bulk C and N contents and C/N ratios of the parent bodies of iron meteorites

Thermal models simulating the evolution of the parent bodies of magmatic irons (fuelled by ^{26}Al decay) predict that the deeper interiors of planetesimals underwent large-scale melting beneath unmolten outer layers (Hevey and Sanders, 2006; Sahijpal et al., 2007; Lichtenberg et al., 2016; Kaminski et al., 2020; Sturtz et al., 2022). Therefore, unlike large rocky planets that had episodes of surficial magma oceans (MOs) during collisionary growth, core-mantle differentiation in the parent bodies of magmatic irons took place in sub-surficial MOs. Following the framework of Grewal et al. (2022a), the estimated bulk C and N inventories of the parent cores of magmatic irons in the previous sub-section were combined with the relevant metallic melt-silicate melt partition coefficients ($D_C^{metal/silicate}$ and $D_N^{metal/silicate}$, respectively) to estimate the bulk C and N contents of the parent bodies using the equation:

$$M_i^{tot} = M_i^{MO} + M_i^{core} \quad (5)$$

where M^{tot}, M^{MO}, and M^{core} represent the mass of an element i (C or N) in the complete parent body, MO, and core, respectively. We used recent parameterizations of $D_C^{metal/silicate}$ (Fischer et al., 2020) and $D_N^{metal/silicate}$ (Grewal et al., 2021b) (both of which account for the effect of S content in the metallic melt), combined with the core/MO mass ratios of the parent bodies of magmatic irons (Hilton et al., 2022), to predict their bulk C and N contents. For relatively shallow MO-like conditions (applicable for planetesimal-sized bodies), $D_C^{metal/silicate}$ and $D_N^{metal/silicate}$ are primarily controlled by the oxygen fugacity (fO_2) of metal-silicate melt equilibration (Dalou et al., 2017; Speelmanns et al., 2019; Grewal et al., 2019a, 2021b, 2021a). Righter et al. (2016) applied metal-olivine-orthopyroxene equilibria to define the fO_2 of metal-silicate melt equilibration between IW–3 and IW–1.5 in two non-magmatic NC iron groups (IAB-MG and IIE). Campbell and Humayun (2005) estimated fO_2 of metal-silicate melt equilibration in IVB group parent body to be IW–1 (based on the abundances of redox sensitive siderophile elements). Given the lack of systematic constraints on the fO_2 of metal-silicate melt equilibration for all groups of magmatic irons, we performed our calculations at an intermediate fO_2 of IW–2.

As C and N are siderophile elements ($D_C^{metal/silicate}$ and $D_N^{metal/silicate}$ > 1), the bulk C and N concentrations in planetesimals are generally lower than those of their cores by a factor of ~5 (Fig. 6a; Table 2). Owing to the very small core mass fraction of the IVB group (0.04; Hilton et al. (2022)), bulk C and N concentrations in its parent body are lower than in its parent core by a factor of ~20. The differences between C and N concentrations of the bulk planetesimals and parent cores decrease with increasing S content of the parent cores because both $D_C^{metal/silicate}$ (~100–1000, except ~2000 in the S-poor IVB core) and $D_N^{metal/silicate}$ (~50–150) values decrease with increasing S content of the metallic melts. The bulk C and N concentrations in planetesimals follow the volatile depletion trend observed in their cores, with IC group being the C- and N-rich endmember and IVA and IVB groups being C- and N-poor endmembers. The C/N ratios of the bulk planetesimals are slightly lower than their parent cores (Fig. 6b; Table 2) because $D_C^{metal/silicate}$ values are somewhat higher than $D_N^{metal/silicate}$ at IW–2. As observed for the C/N ratios of the parent cores, the bulk C/N ratios of volatile-

rich IC group is higher than that of more volatile-depleted irons. It should be noted that, unlike chondrites, planetesimals from the NC and CC reservoirs are not systematically different in C- and N-contents or C/N ratios. Among the chondrites, CC chondrites are C- and N-rich relative to NC chondrites; however our reconstructed parent body compositions show that the IC group parent body is the most C- and N-rich planetesimal despite belonging to the NC reservoir.

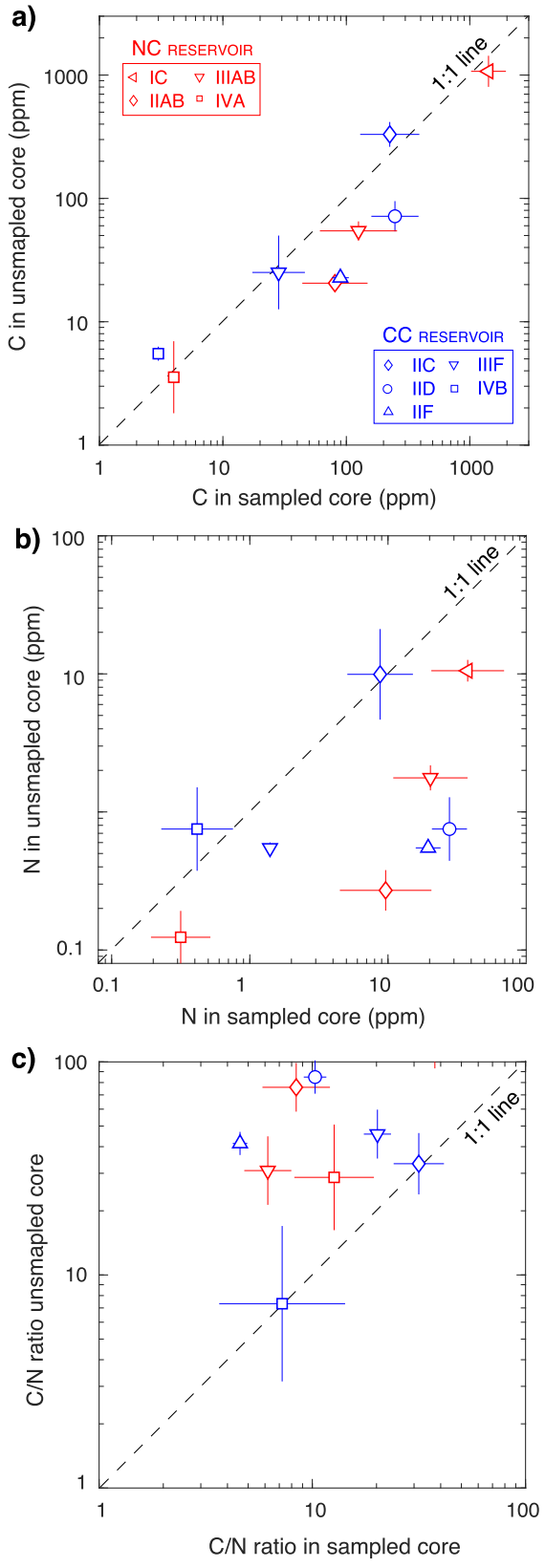

4.3. Comparisons between the C/N ratio of iron meteorites and their parent bodies

The C/N ratios of most of the bulk planetesimals are either similar to or slightly higher than the C/N ratios in grouped iron meteorites (Fig. 7). The exceptions are parent bodies of the IVB group, with its nearly S-free core, and of the IC group, which has a substantially higher C/N ratio than the IC iron meteorites themselves. For most magmatic iron meteorite groups, the meteorites sample the fractional crystallization sequence of the parent core nearly to completion; therefore, the C/N ratios of the parent cores and bulk planetesimals do not differ substantially from that measured directly in the iron meteorites from those groups. However, a large fraction of the IC parent core crystallization sequence is missing from the meteorite record and the IC parent core had an especially high S content. Together these effects lead us to estimate that the parent core and the bulk parent planetesimal of the IC group had a C/N ratio substantially higher than that observed in the IC iron meteorites. The inferences reached in this study (summarized in Fig. 7) depend not only on the experimentally measured solid/liquid metal and metal/silicate partition coefficients for C and N but also on (1) C and N contents measured in different groups of iron meteorites and (2) fractional crystallization models of parent cores (which in turn depend trace element data in iron meteorites and solid/liquid metal partition coefficients for siderophile trace elements). Hence, future constraints from more sophisticated models of fractional crystallization and from better and more numerous measurements of C and N contents in iron meteorites may warrant revisions to our conclusions. Nevertheless, the experimental data and theoretical approach presented in this study will remain essential constraints on such revised interpretations.

4.4. Comparisons between the bulk carbon and nitrogen contents of chondrites and the parent bodies of iron meteorites

Our data constrains the C and N inventories of the parent cores and the entire parent bodies of the earliest formed planetesimals in the NC and CC reservoir (Table 2). The parent bodies of iron meteorites are considerably depleted in C and N compared to chondrites (Fig. 8a). For example, bulk C and N concentrations in the parent body of IC group (volatile-rich iron meteorite group) are ~1–2 orders of magnitude lower than ECs and CI chondrites (best representatives of primitive materials in NC and CC reservoirs), respectively. Bulk C and N contents of the parent bodies of IVA and IVB groups are ~4–5 orders of magnitude lower than those of ECs and CI chondrites. Carbon and nitrogen concentrations are correlated across chondritic groups from both NC and CC reservoirs (Fig. 8a). Consequently, the mean C/N ratios of all chondrites lie in a narrow range (7–26) (Fig. 8b; Table 2). To this well-

Fig. 4. Comparisons of C and N contents and C/N ratios in the missing fractions of the cores with the sampled fractions. (a) C contents of the missing fractions of the cores are not substantially different from the sampled fractions, since $D_C^{solid/liquid}$ does not vary far from unity in the range of S contents achieved by the missing fractions. (b) N contents of the missing fractions of the cores which were S-rich are considerably lower than the sampled fractions. (c) C/N ratios of the missing fractions of the cores are generally higher than the sampled fractions, especially for the S-rich groups. Error bars represent ±1σ deviation for each group, propagated from the standard deviation of geometric mean concentrations in each group, the sampled and unsampled mass fraction estimates, and the partition coefficient fits.

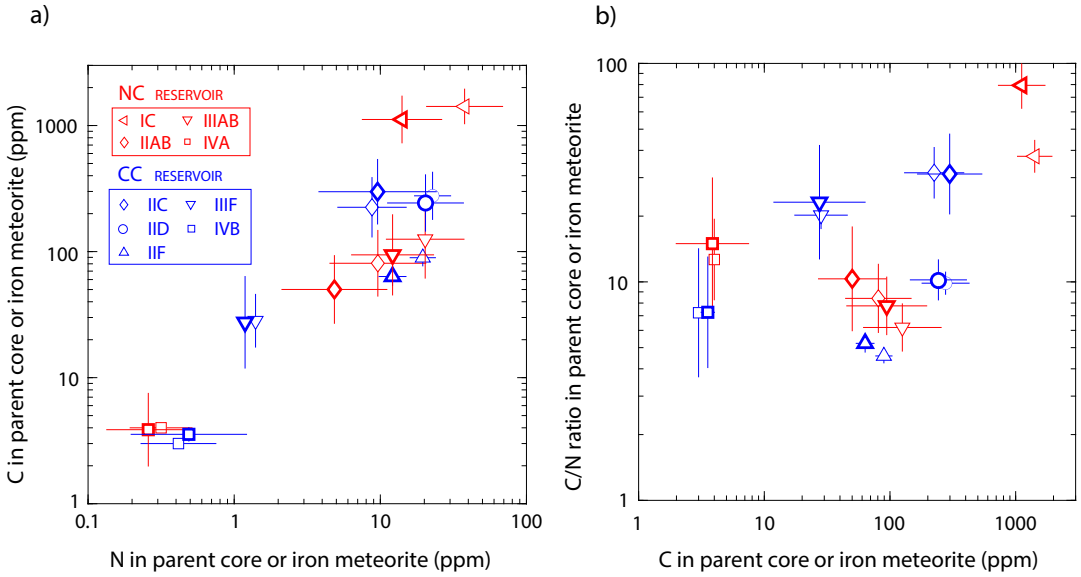

Fig. 5. Comparisons of C and N contents and C/N ratios in the parent cores (bold symbols) with the iron meteorite data (lighter symbols). (a) C contents of the parent cores are similar to the data from iron meteorites, whereas the N contents of the parent cores are generally lower than iron meteorites. (b) C/N ratios of the parent cores are generally higher than those of iron meteorites. Error bars are ± 1-σ uncertainties propagated as in caption to Fig. 4.

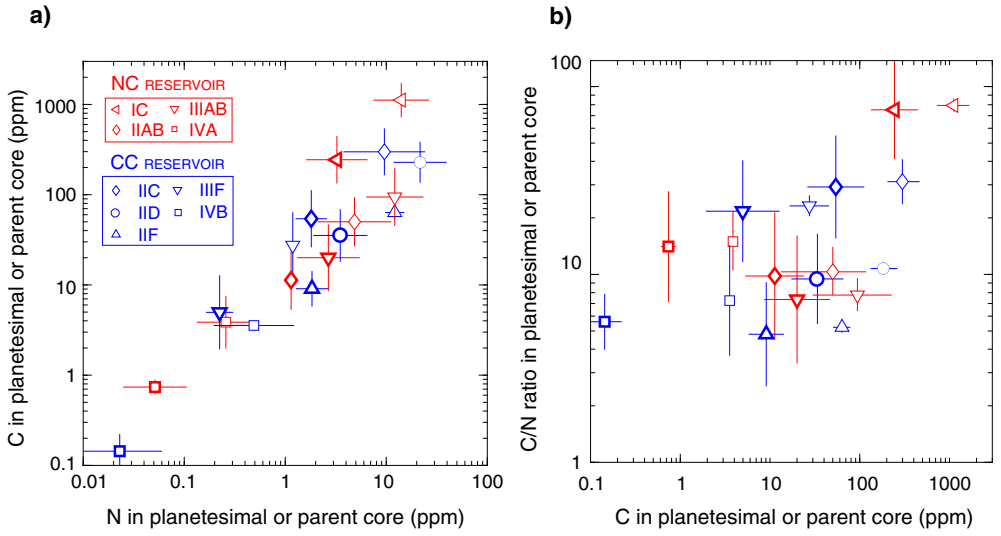

Fig. 6. Comparisons of C and N contents and C/N ratios in the complete parent bodies of iron meteorites (bold symbols) with the same quantities in the cores of those parent bodies (lighter symbols). (a) C and N are both siderophile; the concentrations of each in the complete parent bodies of iron meteorites are approximately a factor of ~5 lower than their concentrations in the cores. (b) However, because C is only somewhat more siderophile than N under appropriate core segregation conditions for these bodies, the C/N ratios in the complete parent bodies of iron meteorites are only slightly lower than those in their cores. Error bars are ±1-σ uncertainties as explained in the caption to Fig. 4 with additional contributions from the metal/silicate partition coefficient uncertainties.

established framework, we now bring the reconstructed parent-body C/N ratios for the differentiated planetesimals. The C/N ratio of the volatile-rich IC group parent body is distinctly higher than that of chondrites. IIC parent body has a C/N ratio that is slightly higher than the chondritic range. C/N ratios of all other groups of iron meteorites are chondritic. Preferential loss of N from the interiors of the planetesimals during thermal metamorphism (prior to sintering temperatures, when the permeability of the interiors is sufficient to allow for efficient volatile loss (Sugiura et al., 1986; Hashizume and Sugiura, 1998)) is necessary to explain the super-chondritic C/N ratios of volatile-rich iron meteorite parent bodies (e.g., IC group). The physical and chemical processes driving such fractionation and loss are currently poorly understood and require further investigation.

The bulk C and N contents in the parent bodies of iron meteorites are offset from the C vs N correlation exhibited by chondrites (Fig. 8a). Except for IIIF, IVA and IVB groups, bulk C contents in the parent bodies decrease without any substantial change in the N contents. This results in a gradual decrease in their C/N ratios from a mean value of 75 in the IC group to 9 in the IIF group (Fig. 8b). Unlike other groups, the N contents of IIIF, IVA and IVB groups decrease with decrease in C contents, so their C/N ratios remain high as they become more C- and N-depleted.

Why are the parent bodies of iron meteorites depleted compared to chondrites? Thermally labile organics were the primary host of C and N in the earliest formed planetesimals (Alexander et al., 1998, 2007; Grewal, 2022). Numerical models predict that substantial amounts of C and N were lost from the interiors of

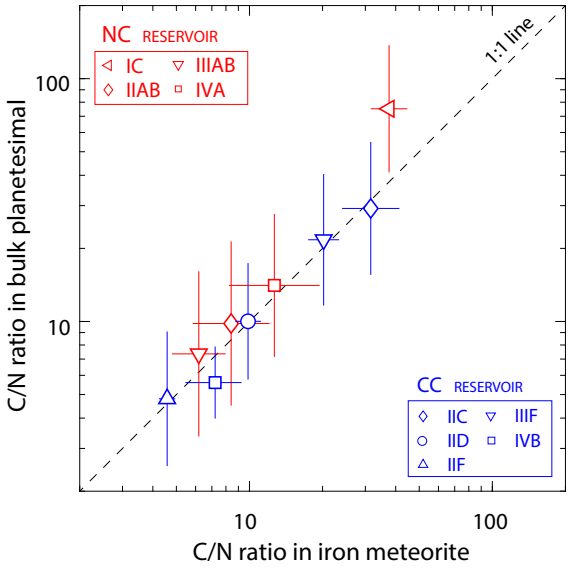

Fig. 7. Comparison of the C/N ratios in the complete parent bodies of iron meteorites with the iron meteorite data. C/N ratios of the parent bodies (except for IVB group) are either similar to or higher than in iron meteorites. Only IC group iron meteorite has a substantially higher C/N ratio in the parent body relative to meteorite samples.

planetesimals during thermal metamorphism fuelled by ^{26}Al decay, resulting in C- and N-depleted interiors prior to the onset of core formation (Sugiura et al., 1986; Hashizume and Sugiura, 1998; Grewal et al., 2022a). If thermal metamorphism explains the C- and N-depleted character of the parent bodies of iron meteorites relative to chondrites, why do C and N concentrations vary among the parent bodies of different groups of iron meteorites? In particular, why are the parent bodies of the IIIF, IVA and IVB groups so depleted in C and N and also in other MVEs like Ge and Ga? The condensation histories of MVEs like Ge and Ga in the protosolar disk are completely decoupled from the formation of organics (the primary carriers of C and N in the primordial materials); therefore, the corelated depletion of MVEs and C and N, starting from IC group and ending with IVA and IVB groups, suggests that variable C and N contents in the parent cores of iron meteorites do not simply reflect accretion of materials with variable amounts of C and N. Indeed, the correlation among chondrites between indices of metamorphism and their C and N contents and N isotope ratios in chondrites is most readily explained if all early-forming planetesimals, independent of their accretion zones, accreted common organic precursors with approximately similar C and N contents (Grewal, 2022; Grewal et al., 2022a). A common degassing event presents the simplest explanation for the common depletion of MVEs, C and N across different groups of iron meteorites. One possibility is vapor degassing from cores that experienced impact disruption of the parent body while still molten, a model that has been invoked to explain large variations in the metallographic cooling rates and Pd-Ag isotope systematics in samples from the strongly volatile-depleted IVA and IVB groups (Yang et al., 2010, 2008, 2007; Hunt et al., 2022; Matthes et al., 2018) and the less volatile-depleted groups IIAB and IIIAB (Hunt et al., 2022; Matthes et al., 2020; Yang and Goldstein, 2006). If the C and N depletion in IIAB, IIIAB, IVA, and IVB groups was a result of core degassing, then the meteorite samples from these groups do not retain the memory of primitive C and N inventories in their parent cores. Consequently, the bulk C and N contents of these and other iron meteorite groups predicted by our model may underestimate the bulk N and C inventories of differentiated planetesimals prior to their disruption and core degassing. This means that the C and N inventories of the earliest formed differentiated planetesimals could have been even higher than those predicted for the volatile-rich IC group (Fig. 8a). Importantly, if the volatile-rich groups like IC retain the most faithful memory of the chemical compositions of their parent core prior to disruption and degassing, then it is likely that the C/N ratios of the earliest formed differentiated planetesimals were at least as high as, if not greater than, the C/N ratio of the IC group (Fig. 8b).

4.5. Implications for the origin of carbon and nitrogen in the BSE

The estimated C and N inventories of the BSE are substantially lower than those of chondrites (Fig. 8a). The N inventory of the BSE, as estimated by Hirschmann (2018) and Marty et al. (2020), lies within the range of bulk N contents in the parent bodies of

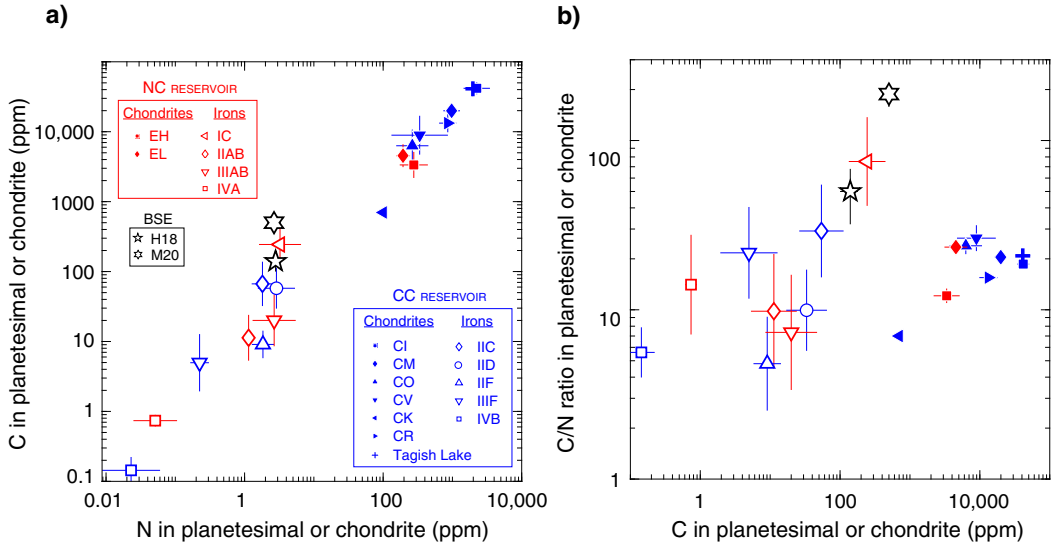

Fig. 8. Comparisons of C and N contents and C/N ratios in the parent bodies of iron meteorites with chondrites and the BSE. (a) C and N contents of chondrites are higher than their abundances in the parent bodies of iron meteorites and the BSE. Note that C content of IC group parent body and N contents of several iron meteorite parent bodies lie within the range of C and N contents of the BSE. (b) The C/N ratio of BSE is higher than that of chondrites and iron meteorite parent bodies, except for the IC parent body. Error bars are ±1σ variation in the reconstruction of each group mean as explained in earlier figure captions.

all groups of irons except for the extremely volatile-depleted IIIF, IVA and IVB groups. By contrast, the bulk C contents of the parent bodies of all groups of irons except the IC group is lower than the estimated C inventory of the BSE. The C content of the IC parent body is higher than the C estimate of BSE by Hirschmann (2018) but lower than that of Marty et al. (2020). We have noted already that the C/N ratios of the BSE estimated by both Hirschmann (2018) and Marty et al. (2020) are higher than those of chondrites (Fig. 8b). The C/N ratio in the group IIC parent body approaches the C/N ratio of the BSE by Hirschmann (2018). The C/N ratio of the IC group parent body is higher than the C/N ratio of the BSE estimated by Hirschmann (2018) but still about a factor of two lower than the Marty et al. (2020) ratio.

Chronological constraints on meteorites combined with numerical models suggest that planetesimal- and planetary embryo-sized bodies began to accrete rapidly (within the timescales of ^{26}Al decay) in the rocky planet forming regions of the protosolar disk (Kruijer et al., 2017; Weidenschilling, 2019; Morbidelli et al., 2022). Consequently, differentiated planetesimals and planetary embryos, and not chondrite-like materials, were the building blocks of the more slowly grown Earth-like rocky planets (Rubie et al., 2011, 2015). We find that the C/N ratios of the parent bodies and parent cores of volatile-rich iron meteorite groups like IC and IIC were superchondritic, while the parent bodies of other volatile-depleted iron groups had C/N within the chondritic range. However, the parent cores of the volatile-depleted groups were either partially or extensively degassed upon parent body disruption (Yang and Goldstein, 2006; Yang et al., 2007, 2008, 2010; Matthes et al., 2018, 2020; Hunt et al., 2022). Therefore, it is likely that the C/N ratios of similar parent bodies that accreted to the Earth rather than being disrupted could also have been as high as those of the volatile-rich groups. This suggests that the seeds of rocky planets likely had superchondritic C/N ratios.

In addition to its superchondritic C/N ratio, the bulk C and N concentrations of the parent body of the volatile-rich IC group is higher than the estimated C and N inventories of the BSE by Hirschmann (2018) but lower than the estimated C inventory of the BSE by Marty et al. (2020) (Fig. 7a). If the C and N inventories of the differentiated planetesimals were even higher than those estimated for the parent bodies of IC group, growth of the Earth from such planetesimals would leave room for the potential segregation of some amount of C and N into the Earth's core during the last stages of its growth and still be able to match the present-day C and N concentrations in the BSE estimated by Hirschmann (2018). This suggests that a C/N ratio for the BSE close to the estimate of Hirschmann (2018) could easily be a natural consequence of the accretion history of our planet. However, a C/N ratio of the BSE closer to the estimate by Marty et al. (2020) would require the accretion of planetesimals with even higher C/N ratios, currently unsampled by the iron meteorite record. If the C and N inventories of the BSE were established by accretion of planetesimals with superchondritic C/N ratios, then the bulk silicate reservoirs of other rocky planets in our Solar System could have similar superchondritic C/N ratios.

5. Conclusions

In this study, we reconstructed the C/N ratios of differentiated planetesimals – the seeds of present-day rocky planets – using iron meteorites as a proxy. Iron meteorites were used to establish C and N contents of the sampled fractions of the parent cores. To estimate C and N contents in the missing fractions of the cores, we conducted high pressure, high-temperature experiments in the Fe—Ni—C—N—S system to constrain the partitioning behavior of C and N between solid and liquid metal during parent core solidification. Our experimental data show that C and N are incompatible in solids relative to S-poor metallic melts but become increasing compatible relative to S-rich metallic melts. Moreover, in S-rich liquids, $D_N^{solid/liquid}$ grows to be almost an order of magnitude higher than $D_C^{solid/liquid}$. This results in higher C/N ratios in the unsampled (S-rich) fractions of the cores than the sampled fractions. As a result, the C/N ratios of parent cores and, in turn, the complete differentiated parent bodies are either similar to or higher than those measured in iron meteorites. The N contents of the iron meteorite parent bodies (except for the most volatile depleted groups) are similar to those of the BSE and the C contents of the parent bodies of volatile-rich groups lie within the range of the BSE estimated by Hirschmann (2018), but lower than the estimate of Marty et al. (2020). Also, C/N ratios of the volatile-rich parent bodies lie within the range of estimates of the C/N ratio of the BSE estimated by Hirschmann (2018), but lower than the estimate of Marty et al. (2020). As iron meteorites from the more volatile-depleted groups likely record the effects of parent core degassing, the C/N ratios of many or perhaps all of the first generation of differentiated planetesimals may have resembled those of the parent bodies of volatile-rich iron meteorite groups. Accretion of such differentiated planetesimals could directly explain the superchondritic C/N ratio of the BSE, if it is closer to the value estimated by Hirschmann (2018), as an initial condition without the need for special loss mechanisms. In light of this evidence, we propose that the superchondritic C/N ratio of the BSE is, contrary to the predictions of previous studies, could be a natural consequence of the accretion history of our planet.

Declaration of Competing Interest

The authors declare that they have no known competing financial interests or personal relationships that could have appeared to influence the work reported in this paper.

Acknowledgements

Thorough, critical, and constructive reviews by Rich Walker and two anonymous reviewers significantly helped improve the clarity of our communication. Mathieu Roskosz is thanked for his efficient handling of the manuscript as the Associate Editor. Amrita P. Vyas is thanked for improving the clarity of our communication. Bidong Zhang and Nicole X. Nie are thanked for insightful discussions related to the formation of iron meteorites. Mike Baker is thanked for the technical support during the experiments. Chi Ma is thanked for his help during the EPMA analyses. Ed Stolper and George Rossman are acknowledged for granting access to their laboratories. This study was funded by a Barr Foundation postdoctoral fellowship by Caltech to D.S.G. Additional support came from NSF award 1911902 to P.D.A.

Appendix A. Supplementary material

The supplementary material file contains information related to the data sources of C and N measurements of iron meteorites used in this study. Additionally, it also includes 2 figures and 3 tables (containing the chemical compositions of starting mixtures, solid metals, and liquid metals). Supplementary material to this article can be found online at https://doi.org/10.1016/j.gca.2023.01.012.

References

Alexander, C.M.O., Bowden, R., Fogel, M.L., Howard, K.T., Herd, C.D.K., Nittler, L.R., 2012. The Provenances of Asteroids, and Their Contributions to the Volatile Inventories of the Terrestrial Planets. Science 337, 721–723.

Alexander, C.M.O.D., Fogel, M., Yabuta, H., Cody, G.D., 2007. The origin and evolution of chondrites recorded in the elemental and isotopic compositions of their macromolecular organic matter. Geochim. Cosmochim. Acta 71, 4380–4403.
Alexander, C.M.O., Russell, S.S., Arden, J.W., Ash, R.D., Grady, M.M., Pillinger, C.T., 1998. The origin of chondritic macromolecular organic matter: A carbon and nitrogen isotope study. Meteorit. Planet. Sci. 33, 603–622.
Bergin, E.A., Blake, G.A., Ciesla, F., Hirschmann, M.M., Li, J., 2015. Tracing the ingredients for a habitable earth from interstellar space through planet formation. Proc. Natl. Acad. Sci. 112, 8965–8970.
Buchwald, V.F., 1975. Handbook of Iron Meteorites: Their History, Distribution, Composition and Structure. University of California Press.
Campbell, A.J., Humayun, M., 2005. Compositions of group IVB iron meteorites and their parent melt. Geochim. Cosmochim. Acta 69, 4733–4744.
Chabot, N.L., 2004. Sulfur contents of the parental metallic cores of magmatic iron meteorites. Geochim. Cosmochim. Acta 68, 3607–3618.
Chabot, N.L., Jones, J.H., 2003. The parameterization of solid metal-liquid metal partitioning of siderophile elements. Meteorit. Planet. Sci. 38, 1425–1436.
Chabot, N.L., Zhang, B., 2022. A revised trapped melt model for iron meteorites applied to the IIIAB group. Meteorit. Planet. Sci. 57, 200–227.
Chabot, N.L., Campbell, A.J., Jones, J.H., Humayun, M., Agee, C.B., 2003. An experimental test of Henry's Law in solid metal-liquid metal systems with implications for iron meteorites. Meteorit. Planet. Sci. 38, 181–196.
Chabot, N.L., Campbell, A.J., Jones, J.H., Humayun, M., Vern, L.H., 2006. The influence of carbon on trace element partitioning behavior. Geochim. Cosmochim. Acta 70, 1322–1335.
Chabot, N.L., Campbell, A.J., McDonough, W.F., Draper, D.S., Agee, C.B., Humayun, M., Watson, H.C., Cottrell, E., Saslow, S.A., 2008. The Fe–C system at 5GPa and implications for Earth's core. Geochim. Cosmochim. Acta 72, 4146–4158.
Chabot, N.L., Drake, M.J., 1997. An experimental study of silver and palladium partitioning between solid and liquid metal, with applications to iron meteorites. Meteorit. Planet. Sci. 32, 637–645.
Chabot, N.L., Saslow, S.A., McDonough, W.F., Jones, J.H., 2009. An investigation of the behavior of Cu and Cr during iron meteorite crystallization. Meteorit. Planet. Sci. 44, 505–519.
Chabot, N.L., Wollack, E.A., McDonough, W.F., Ash, R.D., Saslow, S.A., 2017. Experimental determination of partitioning in the Fe-Ni system for applications to modeling meteoritic metals. Meteorit. Planet. Sci. 52, 1133–1145.
Chen, H., Jacobson, S.A., 2022. Impact induced atmosphere-mantle exchange sets the volatile elemental ratios on primitive Earths. Earth Planet. Sci. Lett. 594, 117741.
Dalou, C., Hirschmann, M.M., von der Handt, A., Mosenfelder, J., Armstrong, L.S., 2017. Nitrogen and carbon fractionation during core–mantle differentiation at shallow depth. Earth Planet. Sci. Lett. 458, 141–151.
Dasgupta, R., Buono, A., Whelan, G., Walker, D., 2009. High-pressure melting relations in Fe-C-S systems: Implications for formation, evolution, and structure of metallic cores in planetary bodies. Geochim. Cosmochim. Acta 73, 6678–6691.
Dasgupta, R., Grewal, D.S., 2019. Origin and Early Differentiation of Carbon and Associated Life-Essential Volatile Elements on Earth. In: Orcutt, B., Daniel, I., Dasgupta, R. (Eds.), Deep Carbon: Past to Present. Cambridge University Press, pp. 4–39.
Dasgupta, R., Walker, D., 2008. Carbon solubility in core melts in a shallow magma ocean environment and distribution of carbon between the Earth's core and the mantle. Geochim. Cosmochim. Acta 72, 4627–4641.
Day, J.M.D., Corder, C.A., Cartigny, P., Steele, A.M., Assayag, N., Rumble, D., Taylor, L. A., 2017. A carbon-rich region in Miller Range 091004 and implications for ureilite petrogenesis. Geochim. Cosmochim. Acta 198, 379–395.
Elkins-Tanton, L.T., Weiss, B.P., Zuber, M.T., 2011. Chondrites as samples of differentiated planetesimals. Earth Planet. Sci. Lett. 305, 1–10.
Fischer, R.A., Cottrell, E., Hauri, E., Lee, K.K.M., le Voyer, M., 2020. The carbon content of Earth and its core. Proc. Natl. Acad. Sci. 117, 8743–8749.
Franchi, I.A., Wright, I.P., Pillinger, C.T., 1993. Constraints on the formation conditions of iron meteorites based on concentrations and isotopic compositions of nitrogen. Geochim. Cosmochim. Acta 57, 3105–3121.
Gaillard, F., Bouhifd, M.A., Füri, E., Malavergne, V., Marrocchi, Y., Noack, L., Ortenzi, G., Roskosz, M., Vulpius, S., 2021. The Diverse Planetary Ingassing/Outgassing Paths Produced over Billions of Years of Magmatic Activity. Space Sci. Rev. 217, 22.
Gaillard, F., Scaillet, B., 2014. A theoretical framework for volcanic degassing chemistry in a comparative planetology perspective and implications for planetary atmospheres. Earth Planet. Sci. Lett. 403, 307–316.
Gibson, E.K., Moore, C.B., 1971. The distribution of total nitrogen in iron meteorites. Geochim. Cosmochim. Acta 35, 877–890.
Goldstein, J.I., Scott, E.R.D., Chabot, N.L., 2009. Iron meteorites: Crystallization, thermal history, parent bodies, and origin. Chem. Erde 69, 293–325.
Goldstein, J.I., Huss, G.R., Scott, E.R.D., 2017. Ion microprobe analyses of carbon in Fe–Ni metal in iron meteorites and mesosiderites. Geochim. Cosmochim. Acta 200, 367–407.
Grewal, D.S., 2022. Origin of Nitrogen Isotopic Variations in the Rocky Bodies of the Solar System. Astrophys J 937, 123.
Grewal, D.S., Dasgupta, R., Holmes, A.K., Costin, G., Li, Y., Tsuno, K., 2019a. The fate of nitrogen during core-mantle separation on Earth. Geochim. Cosmochim. Acta 251, 87–115.
Grewal, D.S., Dasgupta, R., Sun, C., Tsuno, K., Costin, G., 2019b. Delivery of carbon, nitrogen, and sulfur to the silicate Earth by a giant impact. Sci. Adv. 5, eaau3669.
Grewal, D.S., Dasgupta, R., Farnell, A., 2020. The speciation of carbon, nitrogen, and water in magma oceans and its effect on volatile partitioning between major reservoirs of the Solar System rocky bodies. Geochim. Cosmochim. Acta 280, 281–301.
Grewal, D.S., Dasgupta, R., Aithala, S., 2021a. The effect of carbon concentration on its core-mantle partitioning behavior in inner Solar System rocky bodies. Earth Planet. Sci. Lett. 571, 117090.
Grewal, D.S., Dasgupta, R., Hough, T., Farnell, A., 2021b. Rates of protoplanetary accretion and differentiation set nitrogen budget of rocky planets. Nat. Geosci. 14, 369–376.
Grewal, D.S., Dasgupta, R., Marty, B., 2021c. A very early origin of isotopically distinct nitrogen in inner Solar System protoplanets. Nat. Astron 5, 356–364.
Grewal, D.S., Seales, J.D., Dasgupta, R., 2022a. Internal or external magma oceans in the earliest protoplanets – Perspectives from nitrogen and carbon fractionation. Earth Planet. Sci. Lett. 598, 117847.
Grewal, D.S., Sun, T., Aithala, S., Hough, T., Dasgupta, R., Yeung, L.Y., Schauble, E.A., 2022b. Limited nitrogen isotopic fractionation during core-mantle differentiation in rocky protoplanets and planets. Geochim. Cosmochim. Acta 338, 347–364.
Halliday, A.N., 2013. The origins of volatiles in the terrestrial planets. Geochim. Cosmochim. Acta 105, 146–171.
Hashizume, K., Sugiura, N., 1995. Nitrogen isotopes in bulk ordinary chondrites. Geochim. Cosmochim. Acta 59, 4057–4069.
Hashizume, K., Sugiura, N., 1997. Isotopically anomalous nitrogen in H-chondrite metal. Geochim. Cosmochim. Acta 61, 859–872.
Hashizume, K., Sugiura, N., 1998. Transportation of gaseous elements and isotopes in a thermally evolving chondritic planetesimal. Meteorit. Planet. Sci. 33, 1181–1195.
Hevey, P.J., Sanders, I.S., 2006. A model for planetesimal meltdown by 26 Al and its implications for meteorite parent bodies. Meteorit. Planet. Sci. 41, 95–106.
Hilton, C.D., Ash, R.D., Walker, R.J., 2022. Chemical characteristics of iron meteorite parent bodies. Geochim. Cosmochim. Acta 318, 112–125.
Hirschmann, M.M., 2016. Constraints on the early delivery and fractionation of Earth's major volatiles from C/H, C/N, and C/S ratios. Am. Mineral. 101, 540–553.
Hirschmann, M.M., 2018. Comparative deep Earth volatile cycles: The case for C recycling from exosphere/mantle fractionation of major (H_2O, C, N) volatiles and from H_2O/Ce, CO_2/Ba, and CO_2/Nb exosphere ratios. Earth Planet. Sci. Lett. 502, 262–273.
Hirschmann, M.M., Bergin, E.A., Blake, G.A., Ciesla, F.J., Li, J., 2021. Early volatile depletion on planetesimals inferred from C-S systematics of iron meteorite parent bodies. Proc. Natl. Acad. Sci. 118. e2026779118.
Hunt, A.C., Theis, K.J., Rehkämper, M., Benedix, G.K., Andreasen, R., Schönbächler, M., 2022. The dissipation of the solar nebula constrained by impacts and core cooling in planetesimals. Nat. Astron 6, 812–818.
Kaminski, E., Limare, A., Kenda, B., Chaussidon, M., 2020. Early accretion of planetesimals unraveled by the thermal evolution of the parent bodies of magmatic iron meteorites. Earth Planet. Sci. Lett. 548, 116469.
Kerridge, J.F., 1985. Carbon, hydrogen and nitrogen in carbonaceous chondrites: Abundances and isotopic compositions in bulk samples. Geochim. Cosmochim. Acta 49, 1707–1714.
Kothari, B.K., Goel, P.S., 1974. Total nitrogen in meteorites. Geochim. Cosmochim. Acta 38, 1493–1507.
Kruijer, T.S., Burkhardt, C., Budde, G., Kleine, T., 2017. Age of Jupiter inferred from the distinct genetics and formation times of meteorites. Proc. Natl. Acad. Sci. 114, 6712–6716.
Kruijer, T.S., Touboul, M., Fischer-Godde, M., Bermingham, K.R., Walker, R.J., Kleine, T., 2014. Protracted core formation and rapid accretion of protoplanets. Science 344, 1150–1154.
Lewis, C.F., Moore, C.B., 1971. Chemical Analyses of Thirty-Eight Iron Meteorites. Meteoritics 6, 195–205.
Lichtenberg, T., Golabek, G.J., Gerya, T.V., Meyer, M.R., 2016. The effects of short-lived radionuclides and porosity on the early thermo-mechanical evolution of planetesimals. Icarus 274, 350–365.
Marty, B., 2012. The origins and concentrations of water, carbon, nitrogen and noble gases on Earth. Earth Planet. Sci. Lett. 313–314, 56–66.
Marty, B., Almayrac, M., Barry, P.H., Bekaert, D.V., Broadley, M.W., Byrne, D.J., Ballentine, C.J., Caracausi, A., 2020. An evaluation of the C/N ratio of the mantle from natural CO_2-rich gas analysis: Geochemical and cosmochemical implications. Earth Planet. Sci. Lett. 551, 116574.
Marty, B., Zimmermann, L., 1999. Volatiles (He, C, N, Ar) in mid-ocean ridge basalts: Assesment of shallow-level fractionation and characterization of source composition. Geochim. Cosmochim. Acta 63, 3619–3633.
Mathew, K.J., Palma, R.L., Marti, K., Lavielle, B., 2000. Isotopic signatures and origin of nitrogen in IIE and IVA iron meteorites. Geochim. Cosmochim. Acta 64, 545–557.
Matthes, M., Fischer-Gödde, M., Kruijer, T.S., Kleine, T., 2018. Pd-Ag chronometry of IVA iron meteorites and the crystallization and cooling of a protoplanetary core. Geochim. Cosmochim. Acta 220, 82–95.
Matthes, M., van Orman, J.A., Kleine, T., 2020. Closure temperature of the Pd-Ag system and the crystallization and cooling history of IIIAB iron meteorites. Geochim. Cosmochim. Acta 285, 193–206.

Moore, C.B., Lewis, C.F., Nava, D., 1969. Superior Analyses of Iron Meteorites. In: P.M. Millman (Ed.), Meteorite Research. pp. 738–748.
Morbidelli, A., Baillié, K., Batygin, K., Charnoz, S., Guillot, T., Rubie, D.C., Kleine, T., 2022. Contemporary formation of early Solar System planetesimals at two distinct radial locations. Nat. Astron 6, 72–79.
Murty, S.V.S., Goel, P.S., Minh, D.V., Shukolyukov, Y.A., 1983. Nitrogen and xenon in acid residues of iron meteorites. Geochim. Cosmochim. Acta 47, 1061–1068.
Oikawa, H., 1982. Review on Lattice Diffusion of Substitutional Impurities in Iron-A Summary Report 47, 215. Tech. Reports.
Pearson, V.K., Sephton, M.A., Franchi, I.A., Gibson, J.M., Gilmour, I., 2006. Carbon and nitrogen in carbonaceous chondrites: Elemental abundances and stable isotopic compisitions. Meteorit. Planet. Sci. 41, 1899–1918.
Ponganis, K.V., Marti, K., 2007. Nitrogen components in IAB/IIICD iron meteorites. Meteorit. Planet. Sci. 42, 331–346.
Prombo, C.A., Clayton, R.N., 1993. Nitrogen isotopic compositions of iron meteorites. Geochim. Cosmochim. Acta 57, 3749–3761.
Righter, K., Sutton, S.R., Danielson, L., Pando, K., Newville, M., 2016. Redox variations in the inner solar system with new constraints from vanadium XANES in spinels. Am. Mineral. 101, 1928–1942.
Roskosz, M., Bouhifd, M.A., Jephcoat, A.P., Marty, B., Mysen, B.O., 2013. Nitrogen solubility in molten metal and silicate at high pressure and temperature. Geochim. Cosmochim. Acta 121, 15–28.
Rubie, D.C., Frost, D.J., Mann, U., Asahara, Y., Nimmo, F., Tsuno, K., Kegler, P., Holzheid, A., Palme, H., 2011. Heterogeneous accretion, composition and core-mantle differentiation of the Earth. Earth Planet. Sci. Lett. 301, 31–42.
Rubie, D.C., Jacobson, S.A., Morbidelli, A., O'Brien, D.P., Young, E.D., de Vries, J., Nimmo, F., Palme, H., Frost, D.J., 2015. Accretion and differentiation of the terrestrial planets with implications for the compositions of early-formed Solar System bodies and accretion of water. Icarus 248, 89–108.
Sahijpal, S., Soni, P., Gupta, G., 2007. Numerical simulations of the differentiation of accreting planetesimals with 26Al and 60Fe as the heat sources. Meteorit. Planet. Sci. 42, 1529–1548.
Sakuraba, H., Kurokawa, H., Genda, H., Ohta, K., 2021. Numerous chondritic impactors and oxidized magma ocean set Earth's volatile depletion. Sci. Rep. 11, 20894.
Shukla, P.N., Goel, P.S., 1981. Total nitrogen in iron meteorites. Earth Planet. Sci. Lett. 52, 251–258.
Speelmanns, I.M., Schmidt, M.W., Liebske, C., 2019. The almost lithophile character of nitrogen during core formation. Earth Planet. Sci. Lett. 510, 186–197.
Sturtz, C., Limare, A., Chaussidon, M., Kaminski, É., 2022. Structure of differentiated planetesimals: A chondritic fridge on top of a magma ocean. Icarus 385, 115100.
Sugiura, N., Arkani-Hamed, J., Strangway, D.W., 1986. Possible transport of carbon in meteorite parent bodies. Earth Planet. Sci. Lett. 78, 148–156.
Sugiura, N., Fujiya, W., 2014. Correlated accretion ages and ε 54 Cr of meteorite parent bodies and the evolution of the solar nebula. Meteorit. Planet. Sci. 49, 772–787.
Tornabene, H.A., Ash, R.D., Walker, R.J., Bermingham, K.R., 2023. Genetics, age, and crystallization history of group IC iron meteorites. Geochim. Cosmochim. Acta 340, 108–119.
Tsuno, K., Grewal, D.S., Dasgupta, R., 2018. Core-mantle fractionation of carbon in Earth and Mars: The effects of sulfur. Geochim. Cosmochim. Acta 238, 477–495.
Tucker, J.M., Mukhopadhyay, S., 2014. Evidence for multiple magma ocean outgassing and atmospheric loss episodes from mantle noble gases. Earth Planet. Sci. Lett. 393, 254–265.
Wada, T., Wada, H., Elliott, J.F., Chipman, J., 1971. Thermodynamics of the Fcc Fe−Ni−C and Ni−C alloys. Metall. Mater. Trans. B 2, 2199–2208.
Wang, C., Hirama, J., Nagasaka, T., Ban-Ya, S., 1991. Phase Equilibria of Liquid Fe-S-C Ternary System. ISIJ Int. 31, 1292–1299.
Wasson, J.T., 1999. Trapped melt in IIIAB irons; solid/liquid elemental partitioning during the fractionation of the IIIAB magma. Geochim. Cosmochim. Acta 63, 2875–2889.
Weidendorfer, D., Asimow, P.D., 2022. Experimental constraints on truly conjugate alkaline silicate-carbonatite melt pairs. Earth Planet. Sci. Lett. 584, 117500.
Weidenschilling, S.J., 2019. Accretion of the asteroids: Implications for their thermal evolution. Meteorit. Planet. Sci. 54, 1115–1132.
Weiss, B.P., Elkins-Tanton, L.T., 2013. Differentiated Planetesimals and the Parent Bodies of Chondrites. Annu. Rev. Earth Planet. Sci. 41, 529–560.
Yang, J., Goldstein, J.I., 2006. Metallographic cooling rates of the IIIAB iron meteorites. Geochim. Cosmochim. Acta 70, 3197–3215.
Yang, J., Goldstein, J.I., Scott, E.R.D., 2007. Iron meteorite evidence for early formation and catastrophic disruption of protoplanets. Nature 446, 888–891.
Yang, J., Goldstein, J.I., Scott, E.R.D., 2008. Metallographic cooling rates and origin of IVA iron meteorites. Geochim. Cosmochim. Acta 72, 3043–3061.
Yang, J., Goldstein, J.I., Michael, J.R., Kotula, P.G., Scott, E.R.D., 2010. Thermal history and origin of the IVB iron meteorites and their parent body. Geochim. Cosmochim. Acta 74, 4493–4506.
Zahnle, K., Arndt, N., Cockell, C., Halliday, A., Nisbet, E., Selsis, F., Sleep, N.H., 2007. Emergence of a habitable planet. Space Sci. Rev. 129, 35–78.
Zhang, B., Chabot, N.L., Rubin, A.E., 2022. Compositions of carbonaceous-type asteroidal cores in the early solar system. Sci. Adv. 8, 5781.